Asociación Argentina
de Mecánica Computacional

Mecánica Computacional Vol XXVIII, págs. 23-38 (artículo completo)
Cristian García Bauza, Pablo Lotito, Lisandro Parente, Marcelo Vénere (Eds.)
Tandil, Argentina, 3-6 Noviembre 2009

# RECONSTRUCTION ANALYSIS FOR INVERSE SCATTERING USING THE TOPOLOGICAL DERIVATIVE AND THE BOUNDARY ELEMENT METHOD

**Adrián Cisilino[a], Silja Beck[b] and Sabine Langer[b]**

[a]*INTEMA, Universidad Nacional de Mar del Plata – CONICET. Av. Juan B. Justo 4302, 7600 Mar del Plata, Argentina, cisilino@fi.mdp.edu.ar, http://www.intema.gov.ar*

[b]*Institut für Angewandte Mechanik, Technische Universität Braunschweig, Spielmannstraße 11, 38106 Braunschweig, Germany, http://www.infam.tu-bs.de*

**Keywords:** Acoustics, topological derivative, boundary elements

**Abstract.** It is presented in this work a direct (non-iterative) method for solving the inverse scattering problem using the framework provided by the topological derivative and the boundary element method. The application is based on the topological derivative for scattering problems introduced by Feijóo (2004a).

The method allows imaging the boundary of an impenetrable object immersed in a homogeneous medium by using a set of measurements of the radiated scattering pattern resulting from illuminating the object from different directions. This leads to an optimization problem consisting in the minimization of the mismatch between the measured scattering pattern and the scattering pattern resulting from an impenetrable inclusion placed at a point in the medium. The rate of change of this mismatch with respect to the size of the inclusion is the topological derivative field. Based on the heuristics that the boundary of the object can be assimilated to a group of inclusions, the boundary of the object is identified as the locus defined by the positions of the inclusions resulting in the highest values of the topological derivative.

The computation of the topological derivate requires the pressure solutions of the adjoint and forward problems. The solution of the forward problem is that of the incident wave for a medium without obstacles. On the other hand, the adjoint problem accounts for the difference between the forward solution and the scatter measures in the field around the object. Both, the forward and the adjoint problems can be solved analytically.

Reconstructions are done in this work by using synthetic data produced by means of a three-dimensional boundary element analysis which requires the discretization of the object boundary only. The scatter solutions for a number of measuring points placed circularly around the inclusion are used as input data to compute the adjoint solution referenced in the previous paragraph. The BEM calculations are straight forward since the measuring points can be associated to internal points in the BEM model.

Obtained results allow concluding that the BEM implementation of the method has the potential to further develop and implement algorithms which can improve the quality of the reconstructions. To this end an extended version of the present method can be coupled with the algorithms introduced in previous works for the topological optimization of potential (Cisilino, 2006) and elasticity (Carretero et al, 2008) problems using the topological derivative and BEM.

## 1 INTRODUCTION

The inverse scattering problem consists in determining the shape of an object from measurement data of radiation scattered from the object. A number of methods have been developed to solve this type of shape-reconstruction problems (see Feijóo et al; 2001, 2004b). Most of these methods have the drawback that they are iterative and/or require the computation sensitivity of the cost function, what makes them computationally expensive.

The topological derivative was firstly introduced by Ceá et al (2000) by combining a fixed point method with the natural extension of the classical shape gradient. The basic idea behind the topological derivative is the evaluation of cost function sensitivity to the creation of a hole. The application of the topological derivative for inverse scattering problems was introduced by Feijóo (2004a) who presented a direct (non-iterative) method for the solution of the shape-reconstruction problem.

The direct method allows imaging the boundary of an impenetrable object immersed in a homogeneous medium by using a set of measurements of the radiated scattering pattern resulting from illuminating the object from different directions. This leads to an optimization problem consisting in the minimization of the mismatch between the measured scattering pattern and the scattering pattern resulting from an impenetrable inclusion placed at a point in the medium. The rate of change of this mismatch with respect to the size of the inclusion is the topological derivative field. Based on the heuristics that the boundary of the object can be assimilated to a group of inclusions, the boundary of the object is identified as the locus defined by the positions of the inclusions resulting in the highest values of the topological derivative.

The boundary element method (BEM) is a powerful tool in computational acoustic analysis. In applying the boundary element method, only a mesh of the surfaces is required, making it easier to use and often more efficient than computing methods such as the finite element method when dealing with very large or infinite homogeneous domains. Besides, the BEM is very attractive to deal with shape and topology optimization problems because of the reduction in the model remeshing effort when compared to domain discretization methods.

The object of this work is to present a combination of BEM computations and the topological derivative approach for solving the inverse scattering problem in acoustics. This work is a first step towards the implementation of topological optimization algorithms like those introduced in previous works for the optimization of potential (Cisilino, 2006) and elasticity (Carretero et al, 2008) problems using the framework provided by the topological derivative and BEM.

## 2 THE FORWARD AND INVERSE SCATTERING PROBLEMS

Following Feijóo (2004a), the setting of the problem is depicted in Figure 1, where $\Omega$ is a homogeneous medium with scatters $\Omega_0$ with boundary $\Gamma_0$. The boundary $\Gamma_s$ is where the measurements of the scattering pattern are obtained and is assumed as circle of radius $R_s$ that encloses all the scatterers.

The so-called forward problem describes the interaction between the medium, scatterers and the incident radiation of a plane sound pressure wave $p_{inc}(x)=e^{i\kappa x\cdot\mathbf{d}}$ with propagation direction $\mathbf{d}$ and wave number $\kappa=\omega/c$ (the relation of the angular frequency $\omega$ to the speed of sound $c$) governed by the Helmholtz equation as follows

$$\nabla^2 p(x)+\kappa^2 p(x)=0 \quad \text{in } \Omega=\mathbb{R}^2\setminus\Omega_0\,, \tag{1}$$

$$\nabla p \cdot \mathbf{n} = 0 \quad \text{on } \Gamma_0, \tag{2}$$

$$\lim_{r\to\infty} \sqrt{r}\left(\frac{\partial p_s}{\partial n} - i\kappa p_s\right) = 0 \tag{3}$$

where $p$ is the total wavefield given by the addition of the incident and scattered pressured fields, this is $p = p_{inc} + p_s$ and $i$ the imaginary unit. Equation (2) is the sound-hard boundary condition which means that scatterers are modeled as rigid objects. Equation (3) is the Sommerfeld condition which is valid for the scattered part of the wavefield and implies that only outgoing waves are allowed at infinity. It is assumed that there is no attenuation in the medium, so Im(κ) = 0.

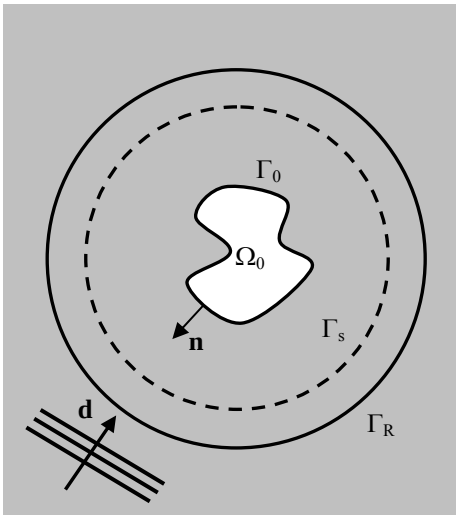


Figure 1: The inverse scattering problem.

At $\Gamma_s$ measurements of $p$ are obtained for different directions $\mathbf{d}_i$ of the incident wave, which will be denoted as $p_m(\mathbf{d}_i)$ (in the following development, $\mathbf{d}_i$ will be dropped to simplify the notation). The objective of the inverse problem is to determine the shape of the scatterers $\Omega_0$ such that $p\big|_{\Gamma_s} = p_m$. This last condition is enforced via a least-squares-type solution of the form:

find $\widehat{\Omega}$ such that

$$\widehat{\Omega} = \arg\min\left(\Omega\right) \tag{4}$$

where

$$J\left(\Omega\right) = \frac{1}{2}\int_{\Gamma_s} \left|p - p_m\right|^2 d\Gamma \tag{5}$$

where $p$ is the solution of Eq. (1)–(3). Thus, the inverse problem is now written in the form of a constrained optimization problem with Ω as the design variable and the forward problem in Eq. (1)–(3) as a constraint on the admissible scalar field $p$.

The strategy to solve the above problem starts from a domain that contains no scatterers. Then, the functional in Eq. (5) is changed to account for the modification of the domain by

introducing a small circular hole, $B_\varepsilon(x)$, centered at $x$ of radius ε. The new domain is denoted by $\Omega_\varepsilon = \Omega \setminus B_\varepsilon(x)$ (see Figure 2).

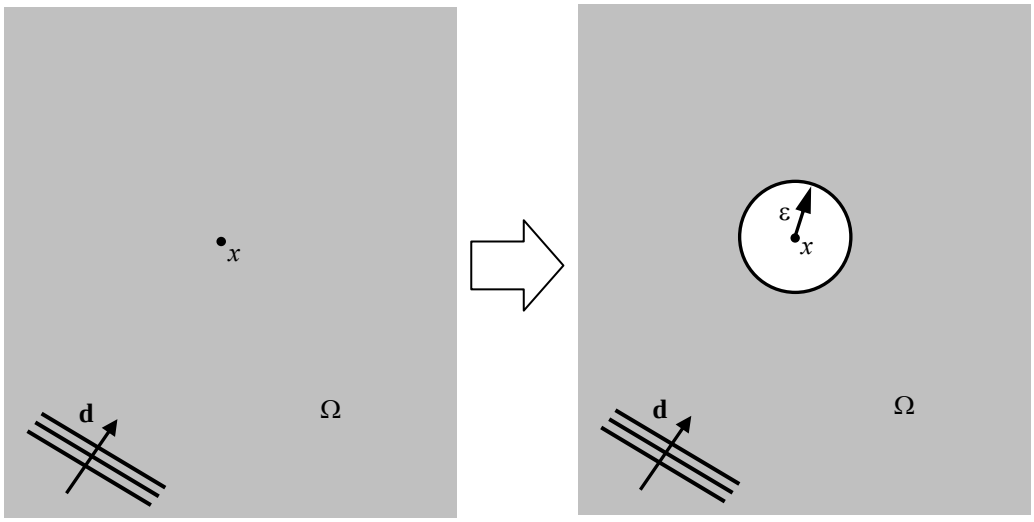


Figure 2: Strategy for the solution of the inverse problem.

Denoting by $f(\varepsilon)$ the negative value of the 'size' of the hole $B_\varepsilon$, the new expression of the functional in Eq. (5) can be expressed as follows:

$$J(\Omega_\varepsilon) = J(\Omega) + f(\varepsilon) D_T(x) + O(f(\varepsilon)) \tag{6}$$

where $D_T(x)$ is the topological derivative which measures the rate of change of the functional value with respect to the size of the scatterer $B_\varepsilon(x)$. The term $O(f(\varepsilon))$ is the remainder and satisfies

$$\lim_{\varepsilon \to 0^+} \frac{O(f(\varepsilon))}{f(\varepsilon)} = 0. \tag{7}$$

The scalar field $D_T(x)$ can be constructed by moving the point $x$ in $\mathbb{R}^2$. Then the reconstruction technique can be motivated as follows: if it is necessary to choose where many small scatterers are to be placed in order to minimize the value of $J(\Omega)$ (and as a consequence recreate the shape of the scatterer by obtaining the scattering pattern that is close to $p_m$), they should be placed where $D_T$ attains high values.

## 3 THE TOPOLOGICAL DERIVATIVE

The topological derivative $D_T(x)$ measures the sensitivity of a shape functional when an infinitesimal 'hole' is subtracted from the domain. This is defined through the following limit:

$$D_T(x) = \lim_{\varepsilon \to 0} \frac{J(\Omega_\varepsilon) - J(\Omega)}{f(\varepsilon)} \tag{8}$$

where $f(\varepsilon)$ is a monotonically decreasing negative function such that $\lim_{\varepsilon \to 0} f(\varepsilon) = 0$. The $f(\varepsilon)$, which corresponds to the size of the 'hole' but not

necessarily is its measure in $\mathbb{R}^2$, is chosen so that $D_T(x)$ is non-trivial, i.e. it satisfies $0 < |D_T(x)| < \infty$.

The direct application and implementation of the concept in Eq. 8 is not straightforward, as it is not possible to establish a homeomorphism between the domains with different topologies (domains with and without the hole). A method for solving the problem using this approach for elasticity can be found in Garreu et al (2001).

Many authors, and in particular Feijoó (2004a) for the case of acoustic problems proposed an alternative definition of the $D_T$ that overcomes the above difficulties. They propose assimilating the creation of a hole to the perturbation of a pre-existing hole whose radius tends to zero (see Figure 3). Therefore, both topologies of the optimization domain are now similar and it is possible to establish a homeomorphism between them. According to this new definition, the expression for the $D_T$ is

$$D_T(x) = \lim_{\substack{\varepsilon \to 0 \\ \delta\varepsilon \to 0}} \frac{J(\Omega_{\varepsilon+\delta\varepsilon}) - J(\Omega_\varepsilon)}{f(\varepsilon+\delta\varepsilon) - f(\varepsilon)} \tag{9}$$

where $J(\Omega_\varepsilon)$ and $J(\Omega_{\varepsilon+\delta\varepsilon})$ are the cost function evaluated for the reference and perturbed domain, $\varepsilon$ is the initial radius of the hole, $\delta\varepsilon$ is a small perturbation of the hole radius and $f$ is a regularization function. The function $f$ is problem dependent and $f(\varepsilon) \to 0$ when $\varepsilon \to 0$.

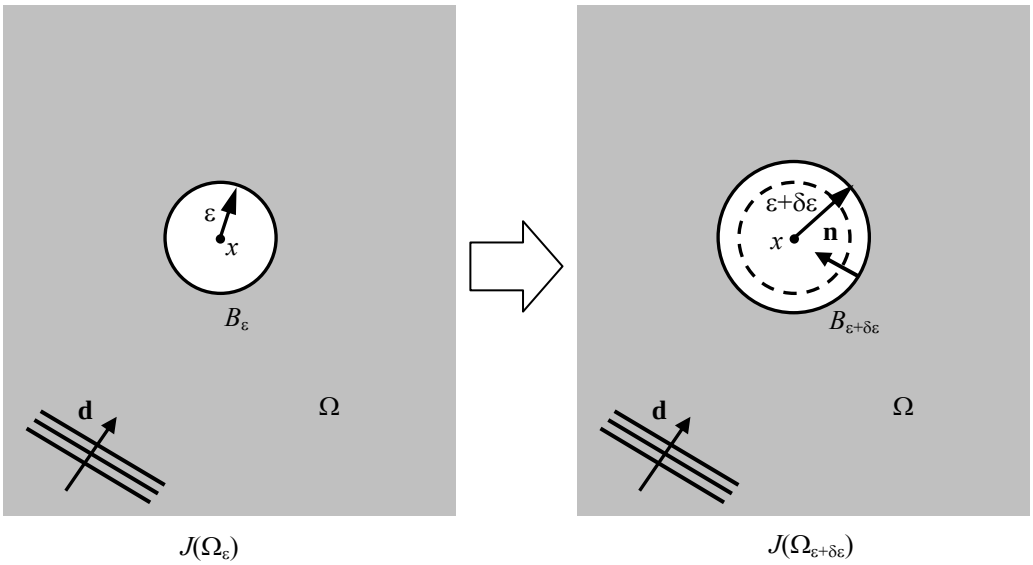


Figure 3: Definition of the topological derivative using the shape sensitivity analysis approach.

It could be argued that the new definition of the $D_T$ in Eq. (9) merely provides the sensitivity of the problem when the size of the hole is perturbed and not when it is effectively created (as it is the case in the original definition of the topological derivative). However, it is understood that to expand a hole of radius $\varepsilon$, when $\varepsilon \to 0$, is nothing more than creating it (a complete mathematical proof that establishes the relation between both definitions of the $D_T$ is given in Novotny et al, 2003). Moreover, the relationship between the two definitions constitutes the formal relation between the $D_T$ and the shape sensitivity analysis. The

advantage of the novel definition for the topological derivative given by Eq. (9) is that the whole mathematical framework developed for the shape sensitivity analysis can now be used to compute the $D_T$.

Among the available shape sensitivity analysis results, the differentiation of the shape derivative for acoustic problems presented by Feijóo et al (2001, 2004b) is of particular interest here. Given a shape functional $J(\Omega)$, the shape derivative $DJ(\Omega)\cdot\mathbf{V}$ in the direction given by the vector field $\mathbf{V}(x)$ is defined as follows:

$$DJ(\Omega)\cdot\mathbf{V}=\frac{d}{d\varepsilon}J\left(\phi_\varepsilon(\Omega)\right)\Big|_{\varepsilon=0} \tag{10}$$

where $\phi_\varepsilon$ is the mapping $\phi_\varepsilon(x)=x+\varepsilon\mathbf{V}(x)$ between the reference and perturbed domains.

The computation of shape derivative in Eq. (10) for the functional $J(\Omega)$ in Eq. (5) in the case in which the direction $\mathbf{V}(x)$ is that of the normal vector **n**(x) (see Figure 3) results in (a detailed derivation of this result is in Feijóo et al, 2004b):

$$DJ(\Omega)\cdot\mathbf{V}=\mathrm{Re}\left[\int_{\Gamma_0}\left(\nabla\lambda^*\cdot\nabla p-\kappa^2\lambda^* p\right)v_n d\Gamma\right], \tag{11}$$

where $p$ is the solution of the forward problem in Eq. (1)–(3) and λ is the solution of the following adjoint problem:

$$\nabla^2\lambda(x)+\kappa^2\lambda(x)=\left(p-p_m\right)(x)\delta_{\Gamma_s}\quad\text{in }\Omega, \tag{12}$$

$$\nabla\lambda\cdot\mathbf{n}=0\quad\text{on }\Gamma_0, \tag{13}$$

$$\lim_{r\to\infty}\sqrt{r}\left(\frac{\partial\lambda}{\partial n}+i\kappa\lambda\right)=0. \tag{14}$$

In Eq. (12), $\delta_{\Gamma_s}$ is the Dirac delta-function defined on the sampling surface $\Gamma_s$. It should be noted that the adjoint field $\lambda$ corresponds to the backpropagation (note the plus sign in Eq. (14) and compare with Eq. (3)) of the mismatch between the solution given by the forward model and the measured signature at $\Gamma_s$.

The topological derivative can be computed now by combining the results in Eq. (9) and Eq. (11). Having in mind that the boundary condition on $\partial B_\varepsilon$ is the one of a rigid object (see Eq. (2)), it results

$$D_T(x)=-\lim_{\varepsilon\to0}\frac{1}{f'(\varepsilon)}\mathrm{Re}\left[\int_{\partial B_\varepsilon}\left(\nabla\overline{\lambda}_\varepsilon\cdot\nabla p_\varepsilon-\kappa^2\overline{\lambda}_\varepsilon p_\varepsilon\right)d\partial B_\varepsilon\right], \tag{15}$$

where $p_\varepsilon$ and $\lambda_\varepsilon$ are solutions of the forward and adjoint problems posed in the configuration $\Omega_\varepsilon=\Omega\backslash B_\varepsilon(x)$ and the symbol $\overline{\ }$ indicates the conjugate complex. An asymptotic analysis of these solutions and their gradients at $\partial B_\varepsilon$ reveals that these terms are of *O(1)* as $\varepsilon\to0$ (see Feijóo, 2004a). Therefore, to satisfy $0<\left|D_T(x)\right|<\infty$ it is required that $f'(\varepsilon)=-2\pi\varepsilon$, which implies that $f(\varepsilon)=-\pi\varepsilon^2$. The final expression for the topological derivative is then

$$D_T(x)=\mathrm{Re}\left[2\nabla\overline{\lambda}(x)\cdot\nabla p(x)-\kappa^2\overline{\lambda}(x)\,p(x)\right], \tag{16}$$

where $p$ and $\lambda$ are solutions of the forward and adjoint problems posed in the configuration

$\Omega_0 = \Omega \setminus B_0(x) = \Omega = \mathbb{R}^2$, this is the domain containing no obstacles.

The forward and adjoint fields in Eq. (16) can be calculated explicitely for the domain with no obstacles. For the forward problem, the solution is that of an incident wave

$$p_{inc}(x) = e^{i\kappa x \cdot \mathbf{d}}. \tag{17}$$

On the other hand, the solution for the adjoint problem in Eq. (12)-(14) for the case of $0 \le r \le R_s$ is given in series (see Feijóo, 2004b)

$$\lambda(r,\theta) = \sum_{n=-\infty}^{n=\infty} A_n J_{|n|}(\kappa r)\varphi_n(\theta), \tag{18}$$

where

$$\varphi_n(\theta) = \frac{1}{\sqrt{2\pi}} e^{in\theta}, \tag{19}$$

$$A_n = +i\frac{\pi R_s}{2} H^2_{|n|}(\kappa R_s) a_n \tag{20}$$

and $a_n$ are the Fourier coefficients of the discrepancy $(p - p_m)(R_s, \theta)$,

$$a_n = \int_0^{2\pi} \varphi_n^*(\theta)(p - p_m)(R_s, \theta) d\theta. \tag{21}$$

## 4 THE BOUNDARY ELEMENT METHOD FOR ACOUSTICS

The Boundary Element Method (BEM) is used in this work to produce synthetic data for the reconstruction algorithm. This is, the BEM is used to compute the $p_m$ along $\Gamma_s$ introduced in the previous sections.

In this work, the direct BEM formulation is used. It is derived for acoustics in the frequency range. The governing equation is the Helmholtz equation, Eq. (22), describing the acoustic pressure distribution in a nonviscous compressible fluid. For unbounded domains Sommerfeld's radiation condition, Eq. (23), must be fulfilled additionally. This condition specifies that waves in an infinite domain only travel into infinity.

$$\nabla^2 p(x) + \kappa^2 p(x) = b(x) \tag{22}$$

$$\frac{\partial p}{\partial n} = i\kappa p + \mathrm{O}\left(\frac{1}{r}\right) \text{ for } r \to \infty \tag{23}$$

where $p$ is the acoustic pressure (the harmonic extention $e^{i\omega t}$ being omitted); $b$ defines a source distribution; the sound flux $\partial p / \partial n$ is the partial derivative of pressure in normal direction and $r$ the distance from the radiating surface.

To apply the BEM for a certain problem two prerequisites have to be fulfilled: the domain is homogeneous and the fundamental solution is known.

### 4.1 Fundamental solution of the Helmholtz-Equation in 3D

The fundamental solution describes the reactions in an unbounded domain caused by a point source with the intensity of 1 at point $\xi$. The fundamental solution $p^*$ needs to fulfill the inhomogeneous differential equation

$$\nabla^2 p^*(x,\xi) + \kappa^2 p^*(x,\xi) = -\delta(x - \xi) \tag{24}$$

with $\delta(x - \xi)$ being the Dirac delta function.

The BEM makes use of the Dirac delta function's property to filter out the value of an

integrand at point ξ:

$$\int_\Omega f(x)\delta(x-\xi)d\Omega = f(\xi). \tag{25}$$

The fundamental solution $p^*$ is the solution of Eq. (24) and becomes for radiation problems with outgoing waves

$$p^*(x,\xi) = \frac{1}{4\pi}\frac{1}{r}e^{i\kappa r} \text{ with } r := |x-\xi|. \tag{26}$$

The fundamental solution solves the homogeneous differential equation for all points $x$ except for the source point ξ where it becomes singular. Differentiation in normal direction gives the fundamental solution for the sound flux:

$$q^*(x,\xi) = -\frac{1}{4\pi}\frac{1}{r^2}(1-i\kappa r)e^{i\kappa r}r_{,n}. \tag{27}$$

Both the fundamental solution and its normal derivative depend on the wave number $\kappa$.

### 4.2 Derivation of the direct boundary integral equation

To derive the boundary integral equation the method of weighted residua is applied to Eq. (22). As test function the fundamental solution (Eq. (26)) is chosen. Applying Green's second identity, resubstituting Eq. (24), and using the filter property of the Dirac delta function leads to

$$p(\xi) = \int_\Gamma \left[q(x)p^*(x,\xi) - p(x)q^*(x,\xi)\right]d\Gamma + \int_\Omega b(x)p^*(x,\xi)d\Omega \text{ for } \xi \in \Omega. \tag{28}$$

The above equation gives the relation for the acoustic pressure $p(\xi)$ at an arbitrary source point within Ω and the boundary functions $p(x)$ and $q(x)$. Moving the source point also onto the boundary Γ yields a relation that only consists of boundary values. To account for the singularity of the fundamental solution at the source point, the source point is considered to be within Ω and enclosed by a sphere-shaped volume of radius ε. Equation (28) is then integrated over two boundary parts $\Gamma - \Gamma_\varepsilon$ and $\Gamma_\varepsilon$ with $\varepsilon \to 0$, leading to the Boundary Integral Equation (BIE)

$$c(\xi)p(\xi) + \int_\Gamma p(x)q^*(x,\xi)d\Gamma = \int_\Gamma q(x)p^*(x,\xi)d\Gamma + \int_\Omega b(x)p^*(x,\xi)d\Omega. \tag{29}$$

The factor $c(\xi)$ is given by

$$c(\xi) = 1 + \lim_{\varepsilon\to\infty}\int_{\Gamma_\varepsilon} q^*(x,\xi)d\Gamma_\varepsilon \tag{30}$$

and becomes $c(\xi) = 0.5$ for a smooth boundary.

### 4.3 Boundary Element Equation

An exact solution of the BIE is generally not available. Therefore, the boundary is discretized into a finite number of boundary elements. The values for acoustic pressure $p$ and flux $q$ are approximated using shape functions in the form of $p = \mathbf{Np}$ and $q = \mathbf{Nq}$, respectively. The vector **N** holds the shape functions while **p** and **q** contain the values of pressure and flux at the nodes. Setting up the BIE, Eq. (29), for each node (collocation method) and assuming for a start that no internal sources are present, leads to a system of equations known as the Boundary Element equation,

$$\mathbf{Gq - Hp = 0}\,. \tag{31}$$

Finally, with known boundary conditions (given flux $\bar{q}$ on a Neumann boundary and given pressure $\bar{p}$ on a Dirichlet boundary) the unknown values for pressure $p$ and flux $q$ can be evaluated. For further details on the boundary element formulation and implementation please refer to any classic book on BEM like Wrobel & Aliabadi (2002).

## 5 THE RECONSTRUCTION ALGORITHM AND VALIDATION EXAMPLE

Figure 4 depicts the set-up for the reconstruction algorithm which was implemented following Feijóo (2004a). The $D_T$ in Eq. (16) is sampled on a grid covering a region of the domain where the object is believed to be located. This requires the computation of the forward and adjoint fields $p$ and $\lambda$ and their gradients. Both the $p$ and $\lambda$ fields and their gradients can be computed analytically using Eqs. (17) and (18), their derivatives. The images generated from this sampling procedure will reveal regions with high values for the topological derivative. These regions are the locations where the boundary of the object may be located. The reasoning behind this heuristic comes from Eqs. (4) and (5), where the inverse scattering problem is identified as an optimization problem, and from Eq. (6): removing regions from $\Omega$ where the topological derivative is high generates a new domain where the cost functional has a lower magnitude and therefore the resulting scattering pattern is closer to the measured signature.

The performance of the algorithm is demonstrated by means of an example consisting in the silhouette of a B2 aircraft (one of the examples presented in the paper by Feijóo, 2004a). Datasets were constructed from 120 measurements obtained along $\Gamma_s$ (this is, a measurement was obtained every 3°). Each dataset corresponds to the illumination of the object by a plane wave with incident direction $\mathbf{d}_i = -\left(\cos\theta_i, \sin\theta_i\right)^T$ with $\theta_i = 2\pi i/120$. The 120 datasets were used to construct the scatters, so $i = 0,1,...119$. The adjoint field given by the series in Eq. (18) was truncated to $n = \pm 30$.

The BEM was used to obtain the $p_m$ measures along $\Gamma_s$. Although the implementation discussed in this work is two-dimensional, a three-dimensional BEM solver was used. The only reason for using the three-dimensional BEM solver is that a two-dimensional one was not available at the moment of preparing this paper. The three-dimensional BEM models in the *x,y,z* domain were assimilated to two-dimensional ones in the *x,y* plane by giving the silhouette of the B2 a dimension in the $\pm z$ directions (see Figure 5). In order to assess possible 3D effects, the B2 shape silhouettes were modeled with thicknesses $z$=±3 m, ±6 m, and ±12 m.

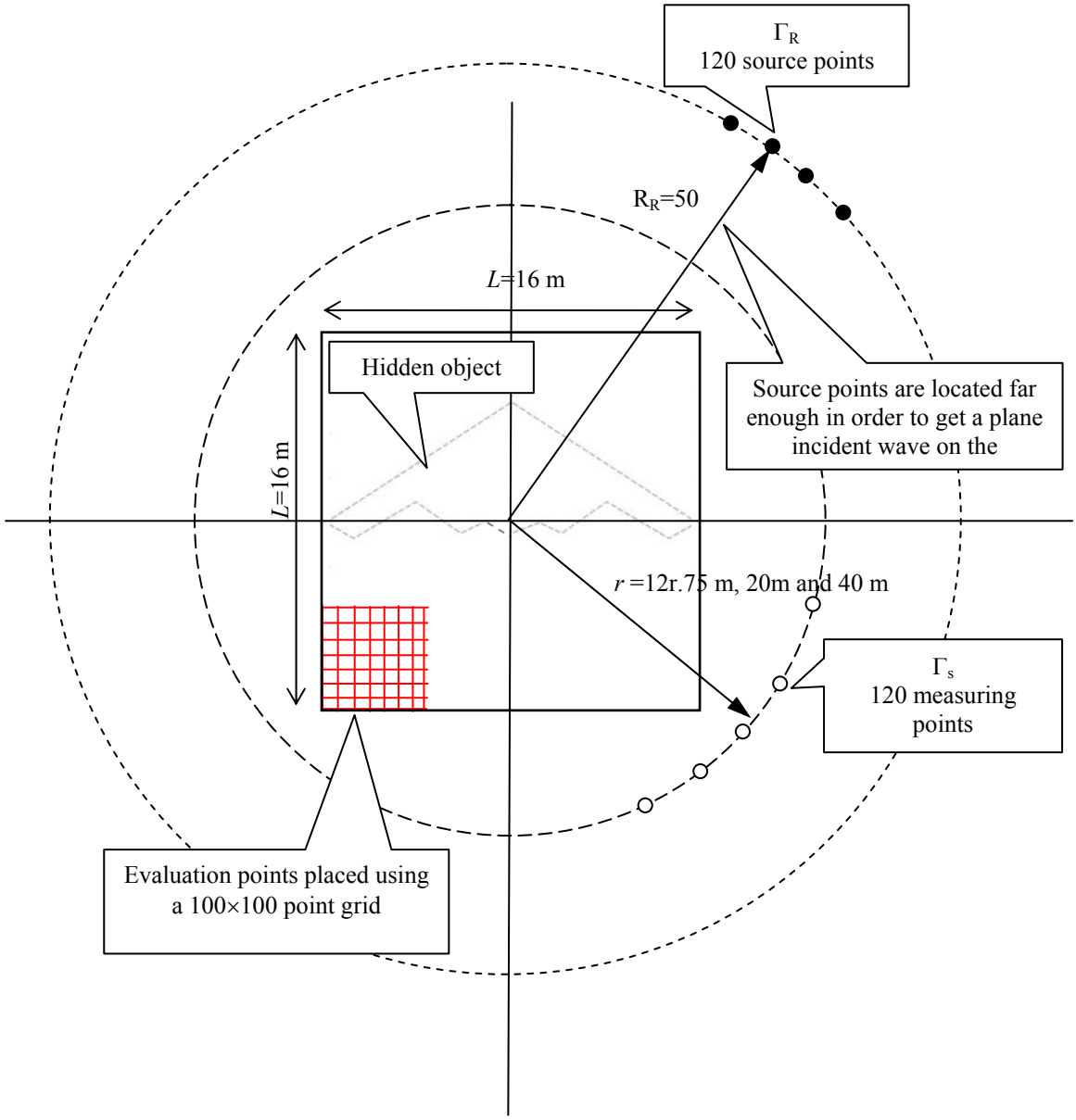


Figure 4: Set-up for the reconstruction algorithm and the solution of the example of the B2 silhouette.

In every case, the sources were placed in the *xy* plane (this is $z$=0) along a circle with a radius $R_R$ =50 m. It is important to note that the implemented BEM code accounts only for point sources; so the position of the sources was set far enough to allow for considering incident waves as plane waves. The surface of the B2 silhouette was modeled as acoustically hard, defining a Neumann boundary with flux $q$ set to zero. Following the paper by Feijóo, 2004a, the ratio between the dimension of the evaluation domain and the wave length was set $L/\lambda$ = 17, the grid spacing was chosen $t=L/100$= 0.16 m, and the ratio of the wave length to the grid spacing $\lambda/t$= 9.375. The wave length was $\lambda$= 1.5 m, the speed of sound $c$= 3 $10^8$ m/s, the source frequency f= 2 $10^8$ Hz and the wave number k= 4.189 1/m. The element size was set to be of maximum value $l$= 0.3 m, thus fulfilling the criterion of the mesh size being one fifth or less of the probing wave length. Models were discretized using quadrilateral linear elements. The model with thickness z=±3 m consisted of 4120 elements, the model with

thickness z=±6 m consisted of 6920 elements and the model with thickness z=±12 m consisted of 12520 elements. Each problem was solved for three positions of the measuring points, for $r$=12.75 m, 20 m and 40 m on the $xy$ plane. Measuring points were assimilated in the BEM model to internal points where the $p_m$ values were computed in a post processing procedure. Models were solved using an AMD Opteron 246, 2.0 GHz CPU. Computation times for a single source point are reported in Table 1. As an example, Figure 6 shows the sound pressure level on the B2 silhouette as well as on the xy plane in the surrounding air with the source placed at 50 m on the x-axis. The sound pressure levels depicted give a typical example for three dimensional distribution including diffraction and interference effects.

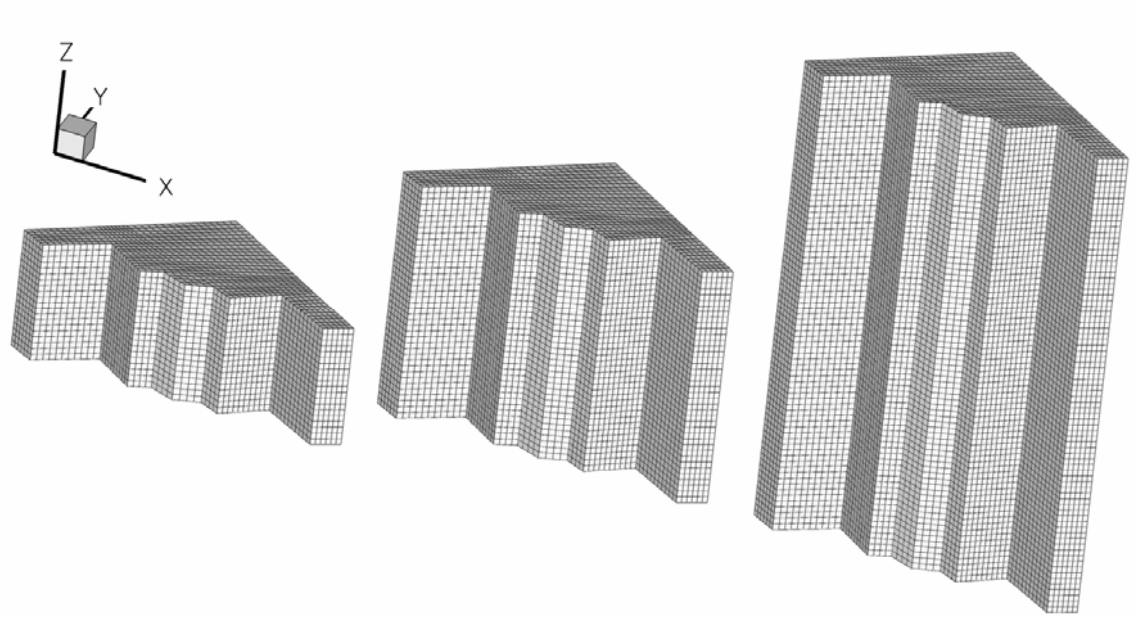


Figure 5: BEM models used to solve the B2 problems. The 2D silhouette in the xy plane was assigned heights of z=±3 m, ±6m, and ±12 m.

| | z=±3 m<br>4120 elements | z=±6 m<br>6920 elements | z=±12 m<br>12520 elements |
|---|---|---|---|
| Computation time | 2:08 min | 7:41 min | 72:39 min |

Table 1: Computation times of the BEM solver

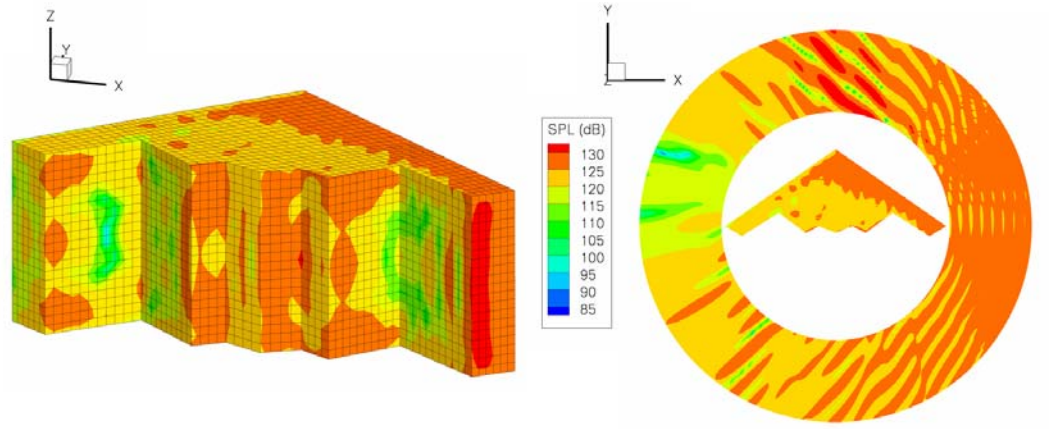


Figure 6: Sound pressure distribution on the B2 structure and on the *xy* plane in surrounding space.

Figures 9, 8 and 7 show the images generated with the topological derivative results resulting from the sampling procedure for the three positions of the measuring points $r$= 40 m, 20 m and 12.75 m. For each case the results are reported for the three thicknesses of the model. The silhouette of the B2 is superimposed (dashed lines). It can be seen that for the cases $r$=12.75 m and 20 m it is possible to make a reasonable reconstruction of the B2 silhouette. For the three sets of results the quality of the reconstruction improves with the model thickness. This allows arguing that three-dimensional effects exist and significantly influence the quality of the calculations. The best result is obtained for the closest position of the measuring points to the object ($r$=12.75 m). This last result was as expected, since the measuring points closest to the object constitute the best scenario for the reconstruction method. Besides, it is worth noting that the closer the measuring points are to the object the ratio $z/r$ increases, and thus it could be argued that the three-dimensional effect is reduced.

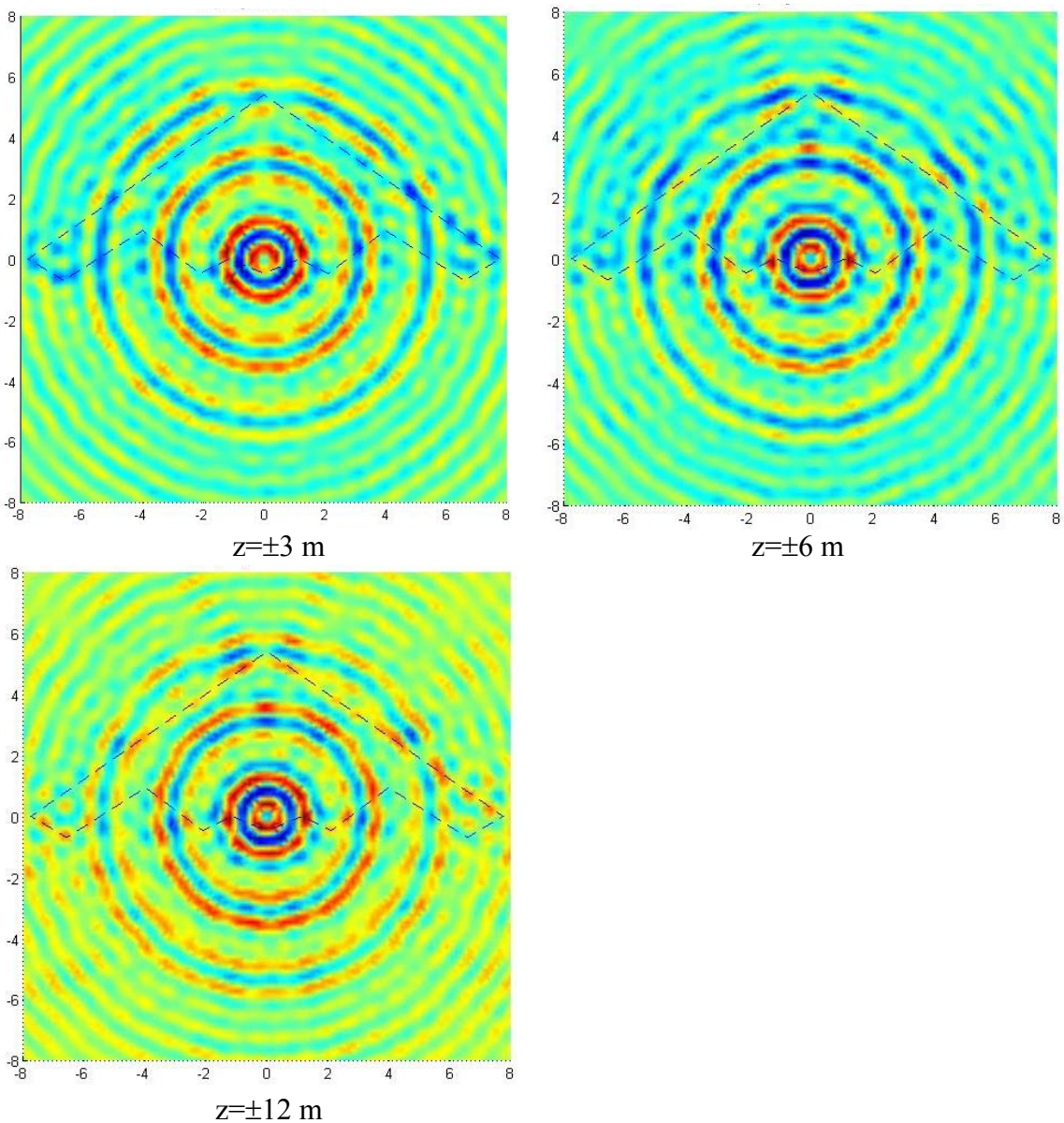


Figure 7: B2 profile superimposed to the topological derivative for the measuring points at $r$=40 m and different thicknesses of the BEM models.

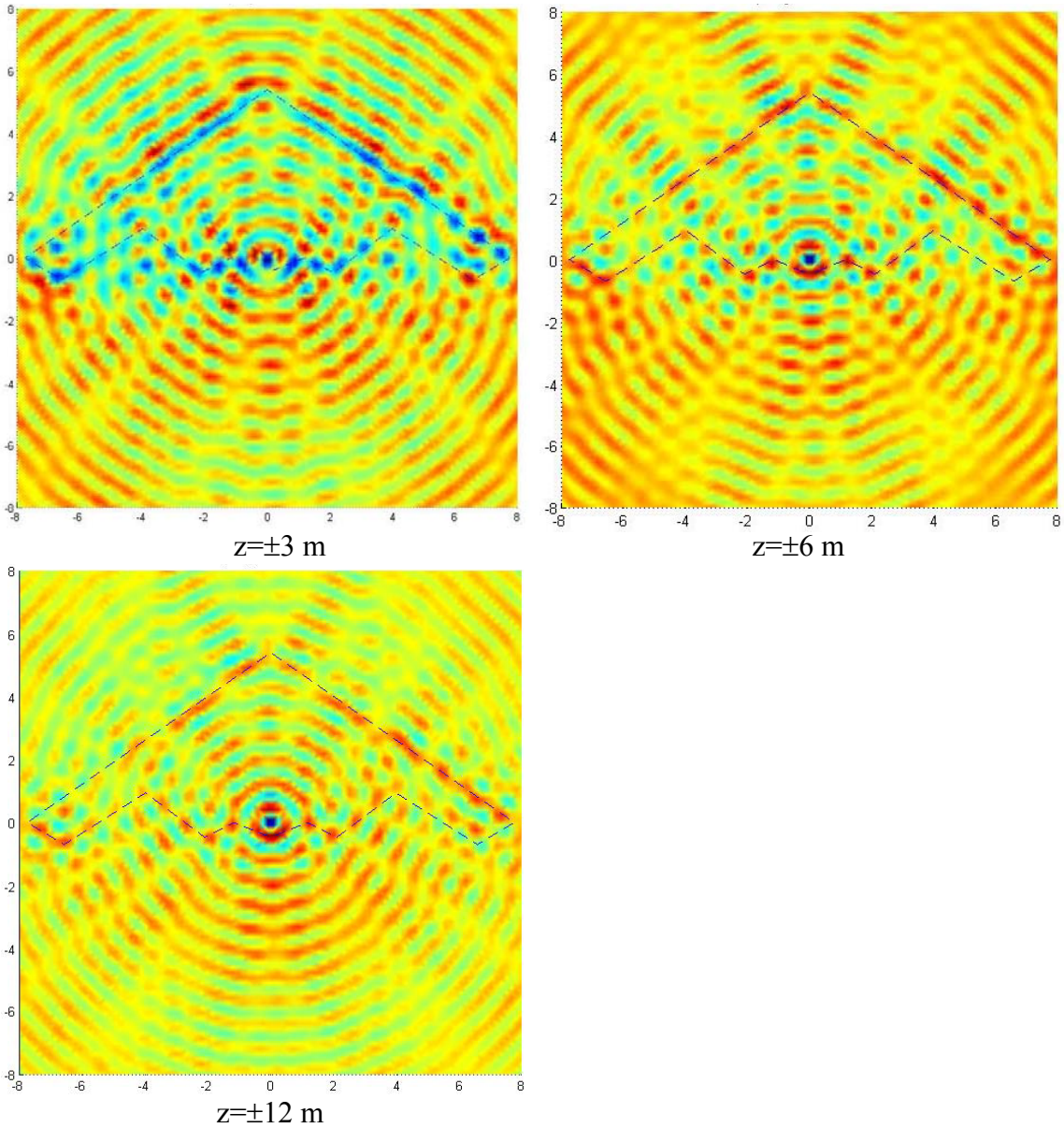


Figure 8: B2 profile superimposed to the topological derivative for the measuring points at $r$=20 m and different thicknesses of the BEM models.

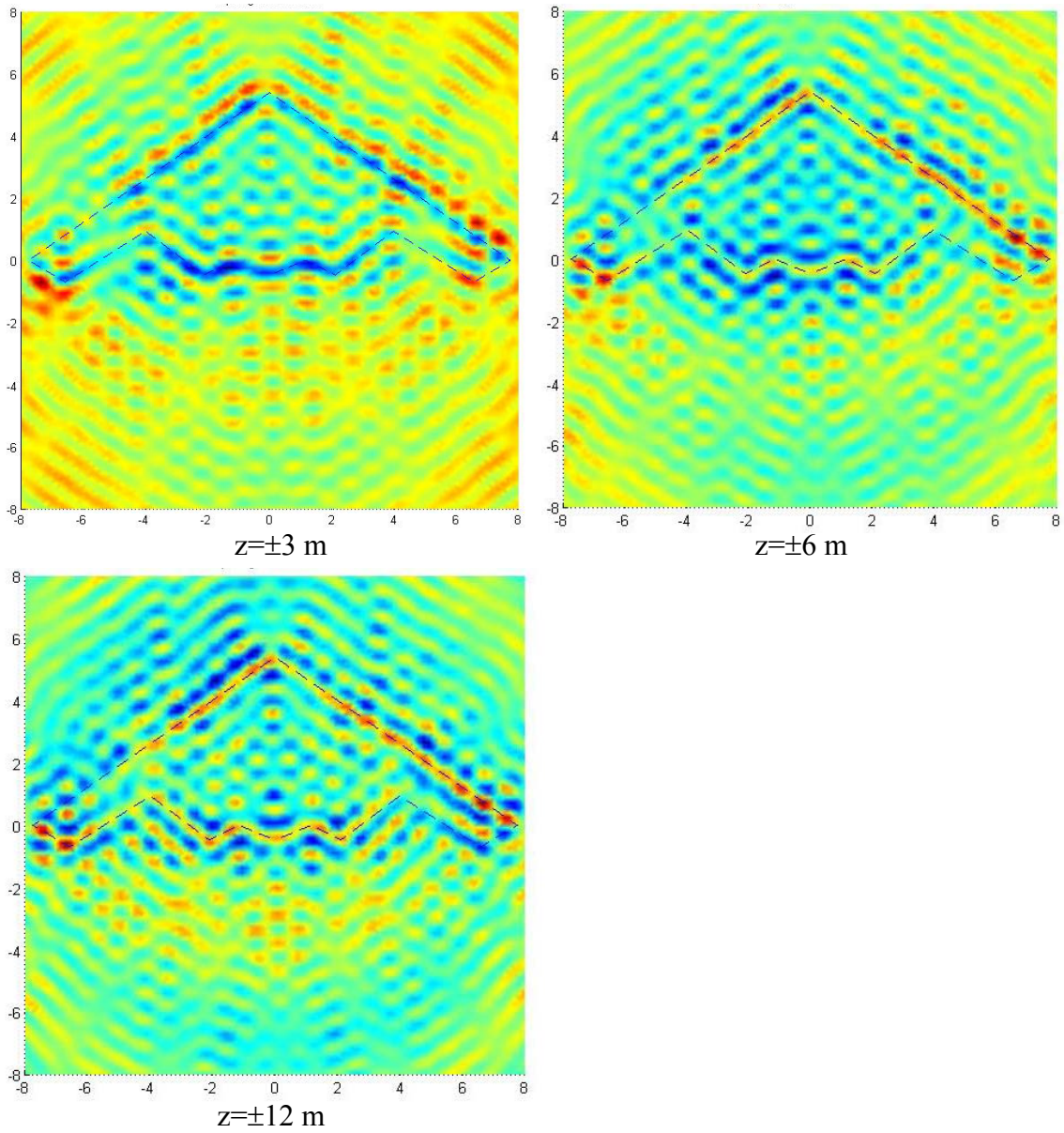


Figure 9: B2 profile superimposed to the topological derivative for the measuring points at $r$=12.75 m and different thicknesses of the BEM models.

## 6 CONCLUSIONS

It has been presented in this work a direct method of a reconstruction algorithm for inverse scattering based on the optimization framework provided by the topological derivative proposed by Feijóo (2004a). The algorithm is very efficient and simple to implement: it involves the computation of a series at points where a function is sampled. Besides, its implementation using BEM for input data is straight forward since the measuring points can be associated to internal points in the model BEM model.

Although the implementation discussed throughout the paper is for two-dimensional problems and plane waves, a three-dimensional BEM solver with point sources was used in this preliminary work. The only reason for using the three-dimensional BEM solver is that a two-dimensional one was not available at the moment of preparing this paper. The three-

dimensional BEM models were assimilated to two-dimensional ones by setting the sources, the measuring points and the evaluation grid in the *xy* plane and by giving the silhouette of the model a thickness in the $\pm z$ direction. The occurring three-dimensional effects were assessed by solving a number of cases with different thicknesses. The point sources were placed far enough from the object in order to assimilate the incident waves to plane ones. The results obtained for the validation examples demonstrate the influence of the three-dimensional effects of the BEM used here.

In spite of the limitations resulting from the utilization of a three-dimensional BEM model to solve the two-dimensional problem, it was possible to obtain reasonable reconstructions when the measuring points were located relatively close to the object. It is concluded that the method has the potential to further develop and implement iterative algorithms which can improve the quality of the reconstructions. To this end an extended version of the present method can be coupled with the algorithms introduced in previous works for the topological optimization of potential (Cisilino, 2006) and elasticity (Carretero et al, 2008) problems using the topological derivative and BEM.

As a further step it is aimed to extend the presented method into a 3D formulation which would allow for reconstruction in space.

## ACKNOWLEDGEMENTS

This work has been supported by the Project DA0806 ‘Acoustic Inverse Scattering Using the Topological Derivative and the Boundary Element Method’ sponsored by the MINCYT (Argentina) and the DAAD (Germany).

## REFERENCES

Ceá J., Garreau S., Guillaume P. and Masmoudi M., The shape and topological optimization connection, *Comput. Methods Appl. Engrg.*, 188:713-726, 2000.

Carretero Neches L. and Cisilino A.P. ,Topology optimization of 2D elastic structures using boundary elements, *Engineering Analysis with Boundary Elements*, 32:533-544, 2008.

Cisilino A.P., Topology optimization of 2D potential problems using boundary elements, *Computer Modelling in Engineering & Sciences*, 15/2:99-106, 2006.

Feijóo G. R., Malhotra M., Oberai A. A. and Pinsky P. M., Shape sensitivity calculations for exterior acoustics problems, *Eng. Comput.*, 18:376–91, 2001.

Feijóo G. R., A new method in inverse scattering based on the topological derivative, *Inverse Problems*, 20:1819-1840, 2004a.

Feijóo G. R., Oberai A. A. and Pinsky P. M., An application of shape optimization in the solution of inverse acoustic scattering problems, *Inverse Problems*, 20:199–228, 2004b.

Garreau S., Guillaume P. and Masmoudi M., The topological asymptotic for pde systems: the elasticity case, *SIAM J. Control Optim.*, 39:1756–78, 2001.

Novotny A.A, Feijoo R.A., Taroco E. and Padra C. C., Topological sensitivity analysis. *Comput. Methods Appl. Mech. Engrg.*, 192:803-829, 2003.

Wrobel L. and Aliabadi M.H., *The Boundary Element Method*, *Applications in Thermo-Fluids & Acoustics*, WileyBlackwell, Volume 1 (2002).